DRAFT VERSION NOVEMBER 27, 2019
Typeset using LATEX **twocolumn** style in AASTeX62

Cluster Difference Imaging Photometric Survey. Vetting Report Description Document

L. G. BOUMA,[1] J. D. HARTMAN,[1] W. BHATTI,[1] J. N. WINN,[1] AND G. Á. BAKOS[1]

[1] *Department of Astrophysical Sciences, Princeton University, 4 Ivy Lane, Princeton, NJ 08540, USA*

ABSTRACT

To find planet candidates in clusters, we make vetting reports using our light-curves (Bouma et al. 2019) and auxiliary data. This document describes the CDIPS planet candidate vetting reports uploaded by `lbouma` to ExoFOP-TESS 2019-09-18 through 2019-11-25.

1. VETTING REPORT DESCRIPTION

The NASA team and MIT teams (Jenkins et al. 2010; Huang et al. 2018) produce vetting reports to assess the quality of planet candidates identified through their transiting planet serach pipelines.

One goal of the CDIPS project is to detect transiting planets with known ages. Therefore our vetting reports include information to help assess *(a)* whether the transiting planet candidate is real, and *(b)* whether the reported age is correct. The code used to make these reports for the 2019-09-18 through 2019-11-25 planet candidates is available online[1].

Figures 1 to 6 summarize the document construed for these purposes. The planet candidate chosen for these figures (Gaia-DR2 `5541111035713815552` = TIC `110718787`) was chosen in part because it passed all the tests. It was reported[2] as a giant planet candidate in an open cluster on Sep 9, 2019. Higher resolution HATSouth photometry revealed about a month afterward that the dip signal comes from a neighboring eclipsing binary.

1.1. *Transit search summary*

Figure 1. Periodograms from TLS and phase-dispersion minimization, calculated with `astrobase.periodbase`, are shown in the top left and top center (Bhatti et al. 2018; Hippke & Heller 2019; Stellingwerf 1978). The top three peaks from each method are shown in the second and third rows; the raw light-curve is in the top-right. A small finder chart from DSS is inset to the top left, with the 1.5-pixel radius aperture used to extract the light-curve in orange.

1.2. *Light-curve diagnostics*

Figure 2. Time-series of raw flux (`IRM2`), TFA-detrended flux (`TF2`), stellar-variability detrended flux, and the background are shown as a function of barycentric Julian date. The overplotted dashed vertical lines are the ephemeris of the highest-power TLS peak from Figure 1. An important visual check is whether the flux dips are correlated with changes in the background level – in this case, they are not. The standard deviation and TESS magnitude are quoted in the upper right. The red line in the second from the top plot is a spline fit, which in this case an essential step for finding the eclipse signal.

The windowed spline is an optional feature: it is only fitted and removed if the star is found to be "variable" (the Lomb-Scargle peak period is found with false alarm probability below 10^{-5}). The spline is a robust penalized B-spline, which is a B-spline with knot-length automatically determined via cross-validation (Eilers & Marx 1996). The idea behind the cross-validation is that more knots leads to smaller residuals on training data, but larger errors when tested on the entire dataset. We used the `wotan` implementation, which is a wrapper to the `pyGAM` spline fitter, with 2σ clipping of outliers from the fit residuals at each iteration (Servén et al. 2018; Hippke et al. 2019). The maximum number of spline knots was set to 50, which for each TESS sector (≈ 25 days) is commensurate with a ≈ 0.5 day window.

1.3. *Transit diagnostics*

Figure 3. The plots show the maximally-detrended light-curve (top); the phase-folded light-curve centered over ± 3 transit durations of the primary transit (middle left); the secondary eclipse (middle right); the odd-numbered transits (lower left); and the even-numbered transits (lower right). The stellar parameters ($T_{\rm eff}, R_\star, M_\star$) are taken from TICv8 when available (Stassun et al. 2019). The first eight lines of text are parameters determined from the best-fitting TLS model. The one exception is the planet radius, which uses the stellar radius as noted above. The "flux contamination" (`TICCONT`) from neighboring stars is *never* taken into account, because transit depth dilution does not affect image subtraction analyses in the same manner as aperture-photometry reductions. The significance of the odd-to-even asymmetry is quoted, but given the strong rotational variability in this object (Figure 2), the apparent odd-even asymmetry could have been caused by the detrending process. To estimate the transit to occulation depth ratio $\delta_{\rm tra}/\delta_{\rm occ}$, the phase-folded light-curve is also fit by a sum of two gaussians (in

Corresponding author: L. G. Bouma
luke@astro.princeton.edu

[1] https://github.com/lgbouma/cdips/tree/a83a30
[2] https://exofop.ipac.caltech.edu/tess/view_ctoi.php

this case, the fit failed). "AstExc" refers to the Gaia-DR2 astrometric excess, which can indicate hints of astrometric binarity in the system. "$d_{\rm geom}$" is the geometric distance from Bailer-Jones et al. (2018). "$R_\star + M_\star \to T_{b0}$" gives the duration of a zero-eccentricity central transit based on the TICv8 stellar radius and mass if available. If the mass is not available, a stellar mass is interpolated from the Pecaut & Mamajek (2013) table, under the assumption that the star is a dwarf.

1.4. *Light-curves for increasing aperture sizes*

Figure 4. Apertures of radius 1, 1.5, and 2.25 pixels are shown from top to bottom. The blue line is the reference transit depth from the best-fitting TLS model. Changes in depth with increasing aperture size can indicate that the source of variability is off-center from the aperture, suggesting a photometric blend.

1.5. *Cluster membership assessment diagnostics*

Figure 5. The star was considered a candidate cluster member by the source(s) listed under "Reference", in this case Cantat-Gaudin et al. (2018). The name used in their catalog in this case was `5599752663752776192`, a Gaia-DR2 identifier, which can be back-referenced to find that Cantat-Gaudin et al. (2018) assigned this star a membership probability in Haffner 13 of just 10%. The base catalog for the plots is chiefly that of Kharchenko et al. (2013), due to its homogeneous parameter determination procedure (particularly for age). If a match to the Kharchenko et al. (2013) catalog is found, then the remaining plots are populated. Top-left shows the parallax, with orange points sampled from the Gaia-DR2 posterior, black points the other cluster members in the Kharchenko catalog, and the blue line the claimed Kharchenko parallax for the cluster. A number of field contaminants in the Kharchenko catalog are visible in this case. Top-right are the Gaia proper motions, where against black points are cluster members from Kharchenko, and the orange is the target star. Bottom-left is the color-magnitude diagram, and bottom-right are the on-sky positions. In the text, `N1sr2` is the number of 1σ cluster members reported by Kharchenko et al. (2013) within the cluster angular radius; $\log t$ is the base-10 logarithm of the age in years; `type` matches the type codes provided by Kharchenko et al. (2013); `K13Note` gives the description of the cluster from Kharchenko et al. (2013), if available. Extra caution must be taken when interpreting this set of plots, since they can only show disagreement between the observed star's properties and those of the listed Kharchenko members (and the latter may be biased).

1.6. *Imaging variability diagnostics*

Figure 6. This page helps diagnose which stars are producing the observed variability. Top-left and top-center are the mean out-of-transit (OOT) and mean in-transit calibrated images (separate from any of our image-subtraction analysis). The OOT images are based on the same number of exposures as the in-transit images and split evenly before and after each transit (following Bryson et al. 2013; Kostov et al. 2019). The yellow star is the target; cyan dots are the flux-weighted centroid of the entire image for each transit event; small red crosses are WCS-projected locations of neighbor stars. Middle-left is the most important subpanel: the difference between the OOT and in-transit mean images. If the variability shown in background map (units: ADU) is off-target, the transit is typically not from the target star. Middle-center is the same, normalized by the uncertainty map. Lower left and lower center show the DSS field in linear and log scales at roughly the same pixel scale as the TESS image, with the 1, 1.5, and 2.25 pixel-radius apertures in blue, orange, and green respectively. The brightness of neighborhood stars is given on the far right. Note the slight coordinate rotation difference between DSS and TESS images; DSS images are aligned north-up, east-left; TESS images are oriented as closely as possible to this system without actually performing the rotation.

2. NEIGHBORHOOD PLOTS

The standard vetting report's neighborhood analysis is helpful, but insufficient for determination of cluster membership. A more thorough approach is to query Gaia-DR2 for nearby stars in position, parallax, and proper motion space, and let the data speak for itself regarding *(a)* the existence of the group, and *(b)* the target star's membership within the group.

For these plots, the "neighborhood" is defined as a group of at most 10^4 randomly selected stars within:

$$\langle\alpha\rangle \pm 5\sigma_\alpha, \quad (1)$$

$$\langle\delta\rangle \pm 5\sigma_\delta, \quad (2)$$

$$\langle\pi\rangle \pm 5\sigma_\pi, \quad (3)$$

where (α, δ, π) are the right ascension, declination, and parallax. $\langle x\rangle$ denotes the mean over all stars within the claimed cluster, σ_x denotes the standard deviation. The limiting G magnitude for the "neighborhood" is set to 18 for Cantat-Gaudin et al. (2018) groups, and 16 for Kharchenko et al. (2013) groups.

For the 2019-09-18 through 2019-11-25 deliveries, these plots were made with code available online[3].

2.1. *Neighborhood diagnostic*

Figure 7 shows the labelled quantities from the target star, the neighborhood, and the "cluster members" reported by either Cantat-Gaudin et al. (2018) or Kharchenko et al. (2013). The top three subplots intentionally omit the labelled cluster members, in order to give the user their own by-eye assessment of whether they see clusters in the neighborhood, and whether the target star is within those clusters.

2.2. *Neighborhood diagnostic, with overplot*

Figure 8. Same as Figure 7, but with overplotted cluster members on the upper three subplots.

[3] https://github.com/lgbouma/cdips_followup/tree/e4d9d

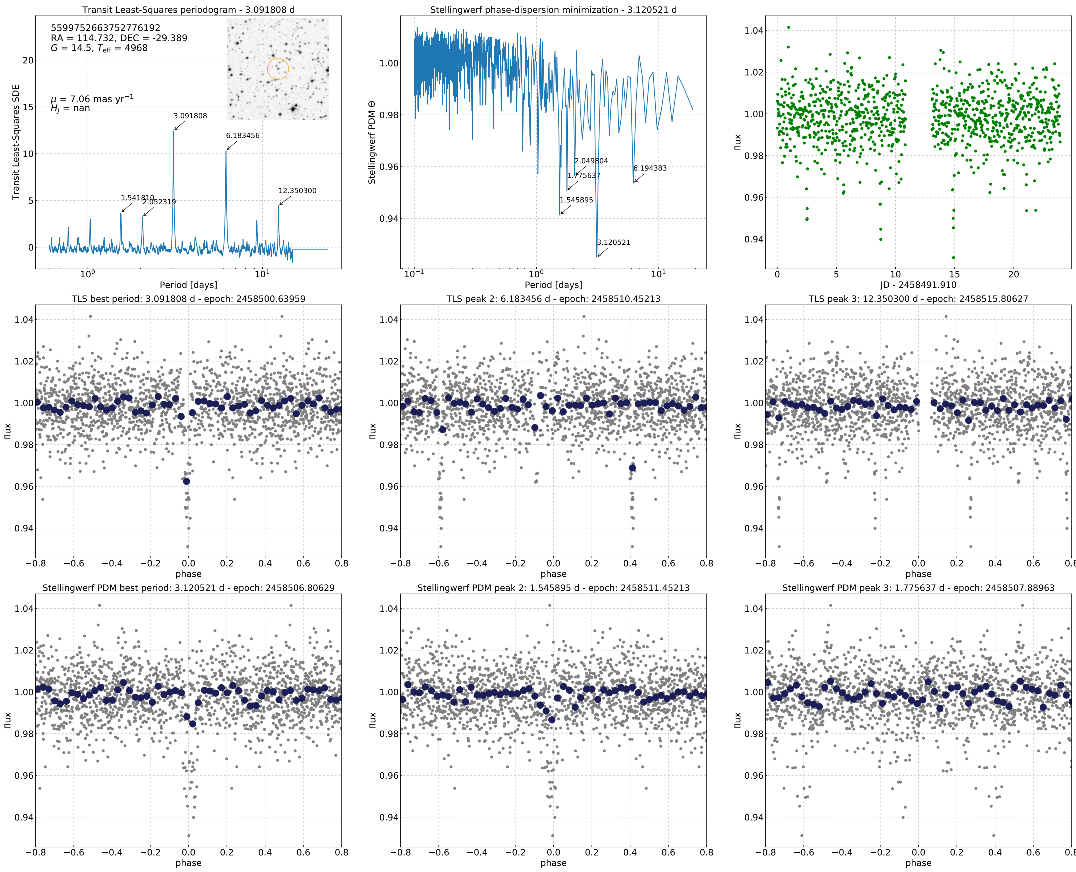

Figure 1. Transit search summary. See § 1.1.

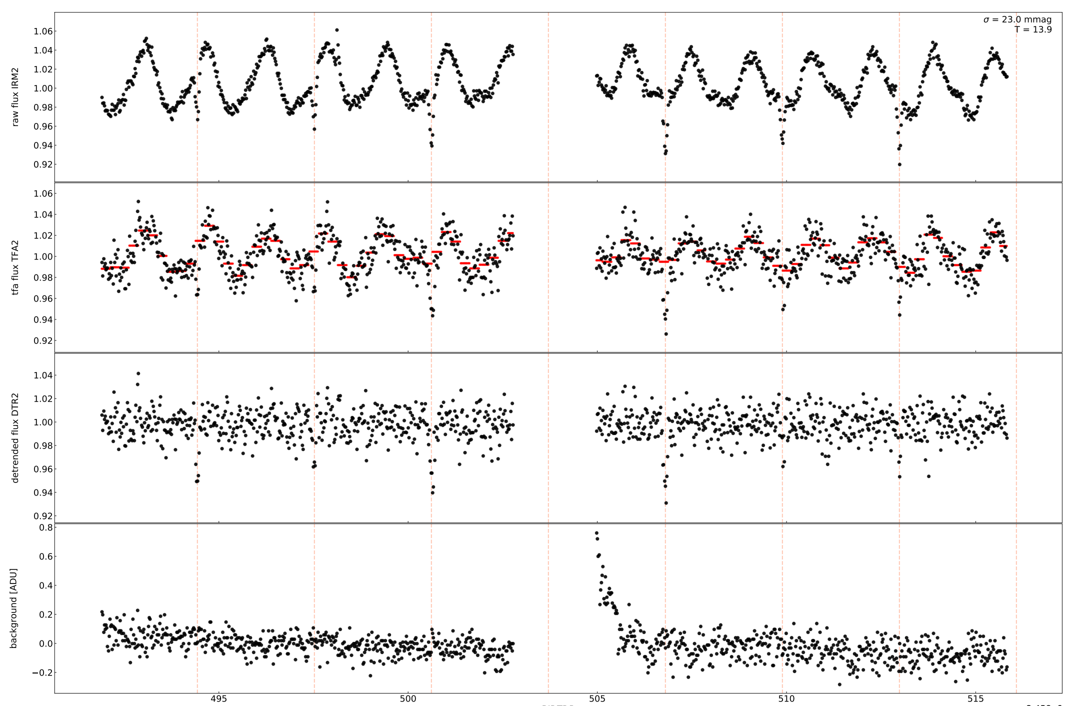

Figure 2. Light-curve diagnostics. See § 1.2.

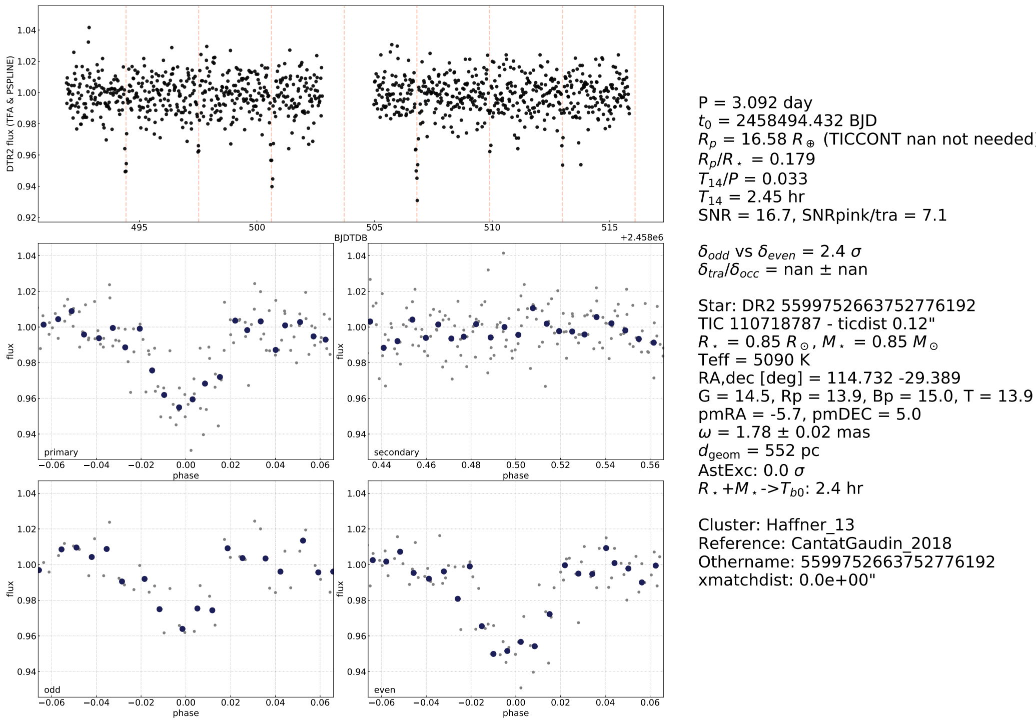

Figure 3. Transit diagnostics. See § 1.3.

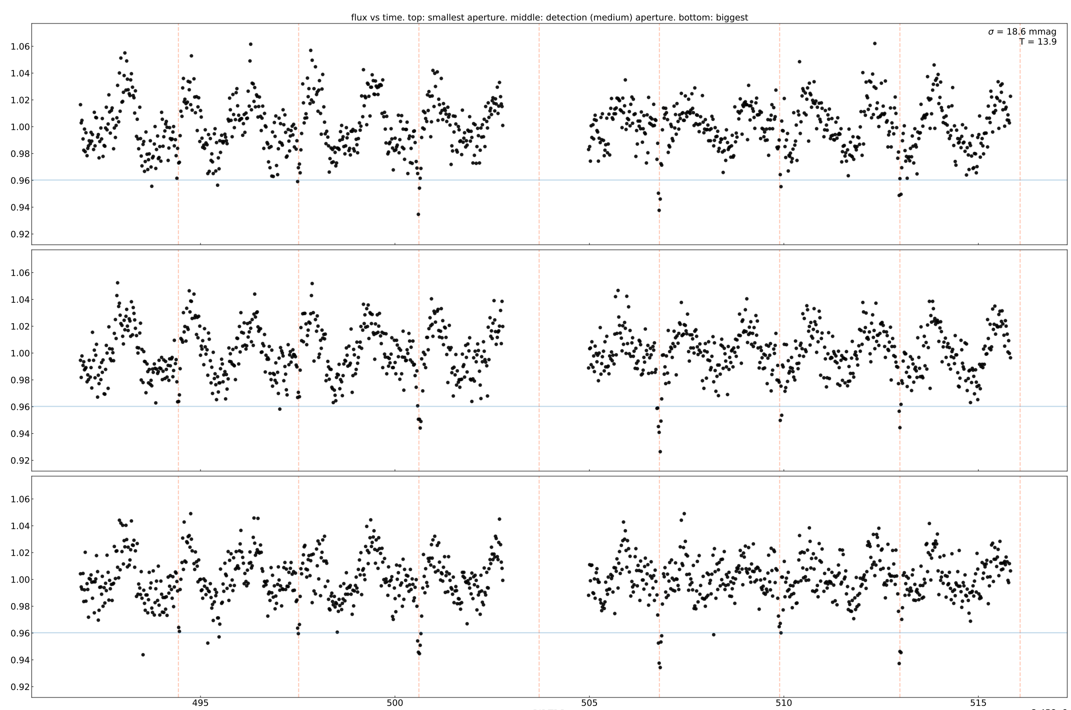

Figure 4. Light-curves for increasing aperture sizes. See § 1.4.

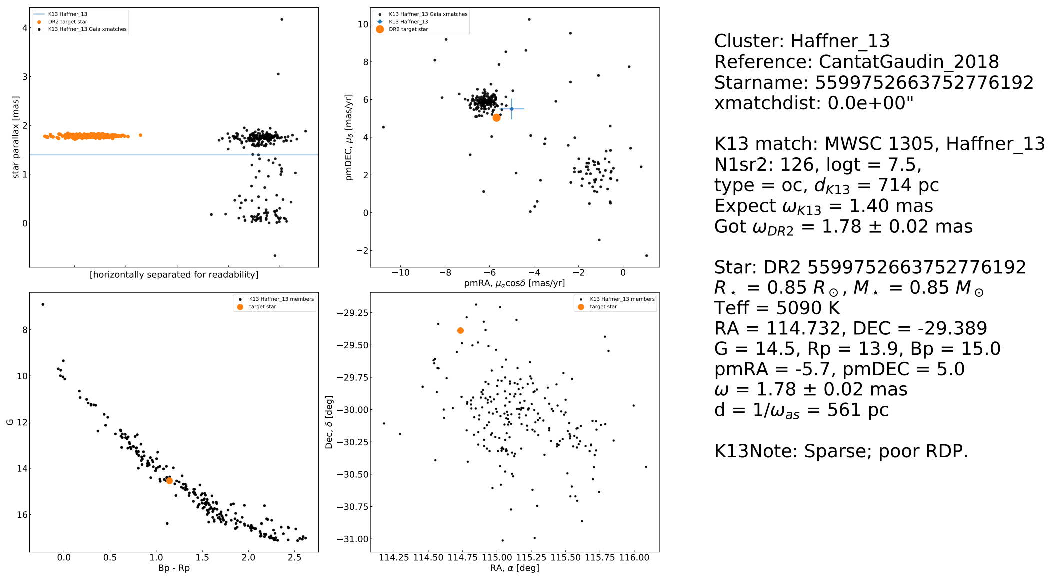

Figure 5. Cluster membership assessment diagnostics. See § 1.5.

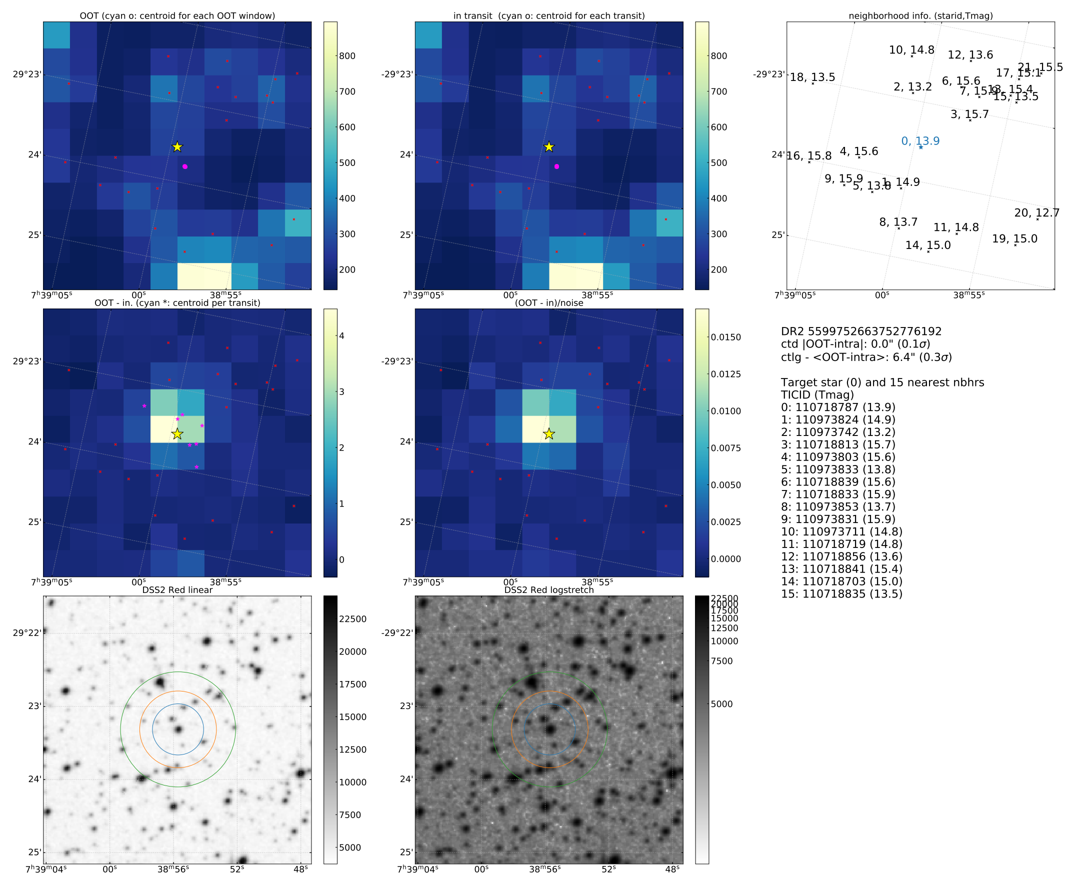

Figure 6. Imaging variability diagnostics. See § 1.6.

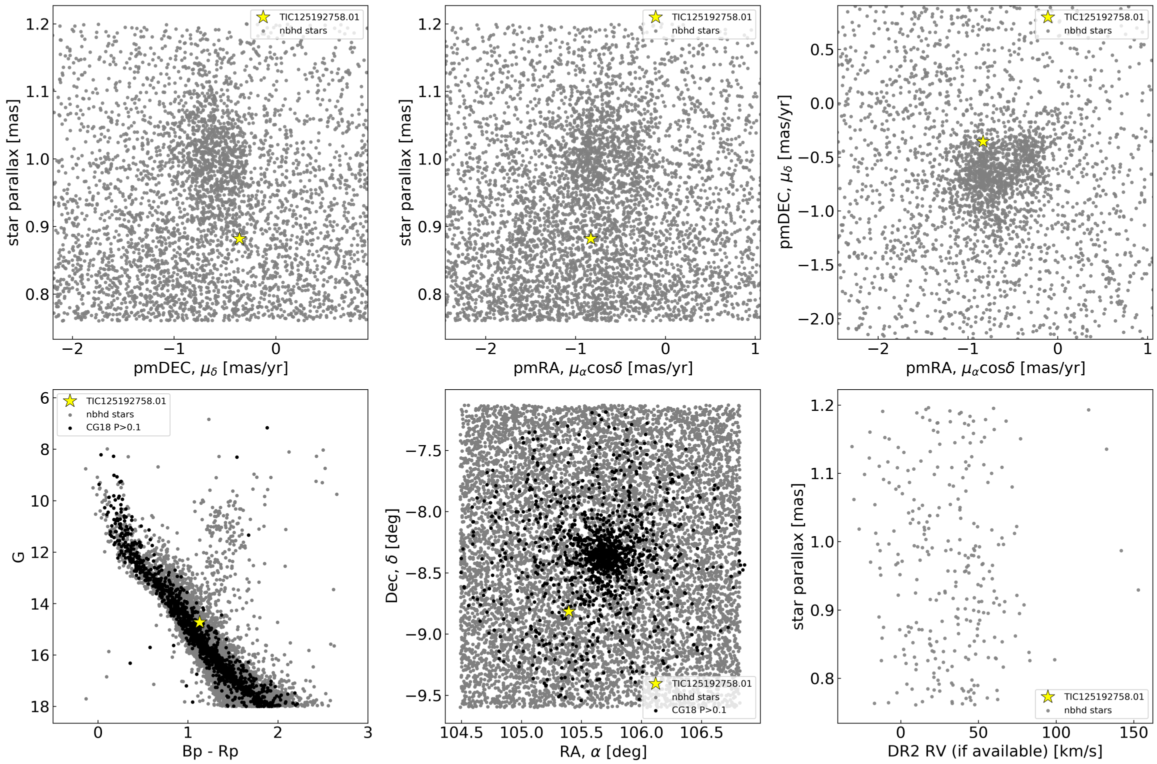

Figure 7. Neighborhood diagnostic. See § 2.1.

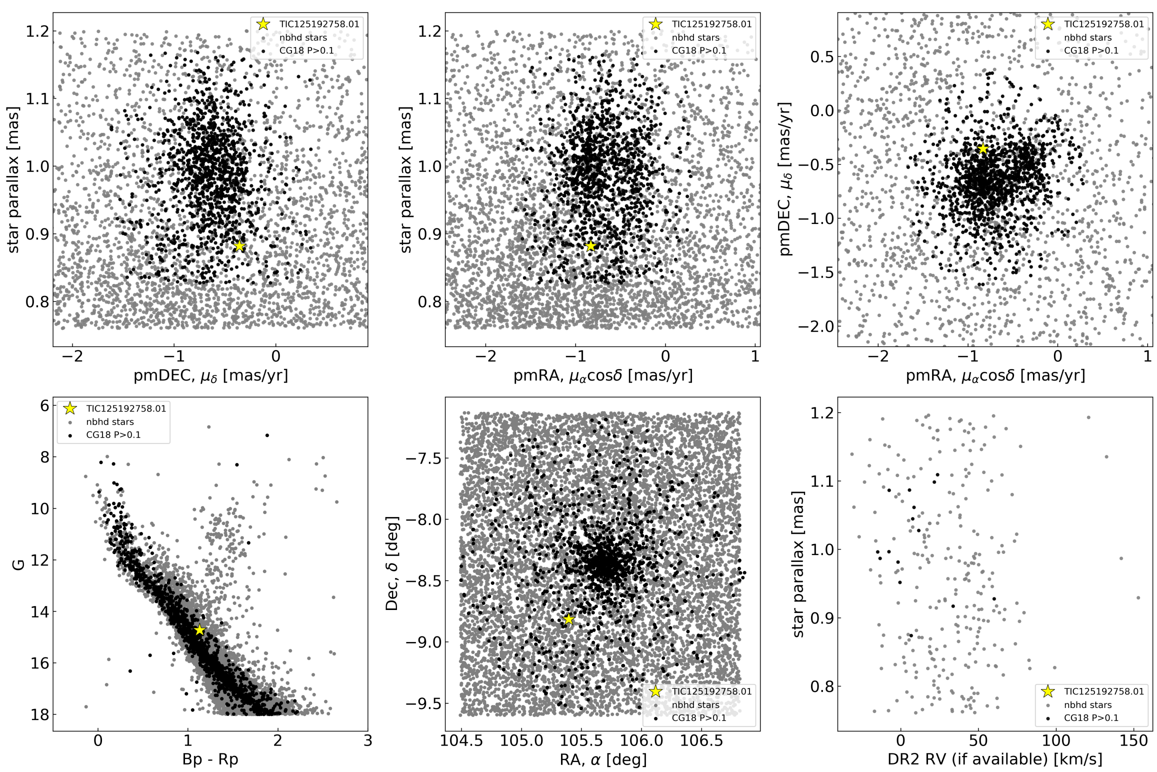

Figure 8. Neighborhood diagnostic with additional overplotted points. See § **??**.

REFERENCES

Bailer-Jones, C. A. L., Rybizki, J., Fouesneau, M., Mantelet, G., & Andrae, R. 2018, arXiv:1804.10121 [astro-ph], arXiv: 1804.10121

Bhatti, W., Bouma, L. G., & Wallace, J. 2018, `astrobase`

Bouma, L. G., Hartman, J. D., Bhatti, W., Winn, J. N., & Bakos, G. Ã. 2019, ApJS, 245, 13

Bryson, S. T., Jenkins, J. M., Gilliland, R. L., et al. 2013, Publications of the Astronomical Society of the Pacific, 125, 889

Cantat-Gaudin, T., Jordi, C., Vallenari, A., et al. 2018, Astronomy & Astrophysics, 618, A93

Eilers, P. H. C., & Marx, B. D. 1996, Statistical Science, 11, 89

Hippke, M., David, T. J., Mulders, G. D., & Heller, R. 2019, arXiv:1906.00966 [astro-ph], arXiv: 1906.00966

Hippke, M., & Heller, R. 2019, arXiv:1901.02015 [astro-ph], arXiv: 1901.02015

Huang, C. X., Burt, J., Vanderburg, A., et al. 2018, The Astrophysical Journal, 868, L39

Jenkins, J. M., Caldwell, D. A., Chandrasekaran, H., et al. 2010, The Astrophysical Journal Letters, 713, L87

Kharchenko, N. V., Piskunov, A. E., Schilbach, E., Röser, S., & Scholz, R.-D. 2013, Astronomy and Astrophysics, 558, A53

Kostov, V. B., Schlieder, J. E., Barclay, T., et al. 2019, arXiv:1903.08017 [astro-ph], arXiv: 1903.08017

Pecaut, M. J., & Mamajek, E. E. 2013, The Astrophysical Journal Supplement Series, 208, 9

Servén, D., Brummitt, C., & Abedi, H. 2018, dswah/pyGAM: v0.8.0

Stassun, K. G., Oelkers, R. J., Paegert, M., et al. 2019, arXiv:1905.10694 [astro-ph], arXiv: 1905.10694

Stellingwerf, R. F. 1978, The Astrophysical Journal, 224, 953